

E2-2015-4

A. Tawfik<sup>1,\*</sup>, A. Diab<sup>1</sup>

TRANSPORT COEFFICIENTS FROM  $SU(3)$   
POLYAKOV LINEAR- $\sigma$  MODEL

Submitted to «Physical Review C»

---

<sup>1</sup> Egyptian Center for Theoretical Physics (ECTP), Modern University  
for Technology and Information (MTI), Cairo, Egypt  
World Laboratory for Cosmology and Particle Physics (WLCAPP),  
Cairo, Egypt

\* <http://atawfik.net/>

Тавфик А., Диаб А.

E2-2015-4

Транспортные коэффициенты в  $SU(3)$  линейной сигма-модели с петлей Полякова

В рамках приближения среднего поля в  $SU(3)$  линейной сигма-модели с петлей Полякова (ЛСМП) проводится изучение большого термодинамического потенциала с целью получения параметров порядка кирального фазового перехода для легких и странных кварков ( $\sigma_l, \sigma_s$ ), а также для изучения параметров порядка деконфайнмента ( $\phi, \phi^*$ ). Кроме того, вычисленный (subtracted) конденсат  $\Delta_{l,s}$  и киральный параметр порядка ( $M_b$ ) сравниваются с результатами решеточной КХД. Используя динамическую модель квазичастиц (ДМКЧ), мы оценили ширину распада и время релаксации для кварков и глюонов. В рамках ЛСМ и с учетом петли Полякова были определены аномалия тензора энергии-импульса ( $\Delta/T^4$ ), удельная теплота и квадрат скорости звука. Кроме того, температурные зависимости нормированной плотности кварков и кварковой восприимчивости были изучены при разных значениях химического потенциала. Электрическая проводимость и теплопроводность,  $\sigma_e$  и  $\kappa$ , объемная и поперечная вязкости,  $\chi$  и  $\eta$ , нормированные к плотности энтропии, оценивались в модели ЛСМП и также сравнивались с данными решеточной КХД.

Работа выполнена в Лаборатории теоретической физики им. Н. Н. Боголюбова ОИЯИ.

Препринт Объединенного института ядерных исследований. Дубна, 2015

Tawfik A., Diab A.

E2-2015-4

Transport Coefficients from  $SU(3)$  Polyakov Linear- $\sigma$  Model

In the mean field approximation, the grand potential of  $SU(3)$  Polyakov linear- $\sigma$  model (PLSM) is analyzed for the order parameter of the light and strange chiral phase-transitions,  $\sigma_l$  and  $\sigma_s$ , respectively, and for the deconfinement order parameters  $\phi$  and  $\phi^*$ . Furthermore, the subtracted condensate  $\Delta_{l,s}$  and the chiral order-parameters  $M_b$  are compared with lattice QCD calculations. By using the dynamical quasiparticle model (DQPM), which can be considered as a system of noninteracting massive quasiparticles, we have evaluated the decay width and the relaxation time of quarks and gluons. In the framework of LSM and with Polyakov loop corrections included, the interaction measure  $\Delta/T^4$ , the specific heat  $c_v$  and speed of sound squared  $c_s^2$  have been determined, as well as the temperature dependence of the normalized quark number density  $n_q/T^3$  and the quark number susceptibilities  $\chi_q/T^2$  at various values of the baryon chemical potential. The electric and heat conductivity,  $\sigma_e$  and  $\kappa$ , and the bulk and shear viscosities normalized to the thermal entropy,  $\xi/s$  and  $\eta/s$ , are compared with available results of lattice QCD calculations.

The investigation has been performed at the Bogoliubov Laboratory of Theoretical Physics, JINR.

Preprint of the Joint Institute for Nuclear Research. Dubna, 2015

## I. INTRODUCTION

One of the main targets of the relativistic heavy-ion facilities such as the Nuclotron-based Ion Collider fAcility (NICA), Dubna, the Relativistic Heavy Ion Collider (RHIC) at BNL, and the Large Hadron Collider (LHC) at CERN is to characterize the phase diagram of hadronic/partonic matter, which can be studied by quantum chromodynamics (QCD) [1, 2], and especially to analyze the properties of the new state of matter, the quark–gluon plasma (QGP) [3], such as the electromagnetic phenomena, which in turn are described by quantum electrodynamics (QED) compared to QCD. Moreover, the predictions of a phase change hadrons/partons by means of lattice QCD calculations assist to complete the view of the experimental and theoretical information about the characteristics of the QCD matter under the extreme conditions of high pressure/density and/or temperature. On the other hand, experimentalists seem to exert a big effort to stimulate the results with as much precision as possible in order to characterize the key properties of such QCD matter in small scale (very high energy). It is obvious that achieving this ultimate goal requires sophisticated theoretical, experimental, and numerical works.

The Polyakov–Nambu–Jona-Lasinio (PNJL) model [4–6], the Polyakov linear- $\sigma$  model (PLSM) or the Polyakov quark-meson model (PQM) [7–10], as well as the Dynamical QuasiParticle Model (DQPM) [11–13] are examples of phenomenological QCD-like models aiming to study the strongly interacting matter in dense and thermal medium. In PLSM, the thermodynamic quantities have been investigated [9, 10, 14, 15]. Furthermore, the normalized and non-normalized higher-order moments of the particle multiplicity have been analyzed within PLSM [10, 15]. Also, the chiral phase-structure of various mesonic states at finite temperatures has been evaluated with and without anomaly contributions [16, 17]. In a previous work, we have presented calculations for the chiral phase-structure of (pseudo)-scalar and (axial)-vector meson masses in thermal and dense medium in presence and absence of the Polyakov loop correction with and without the anomaly contribution [18]. Furthermore, the chiral phase-structure in the limit of large number of colors  $N_c$  and the normalization of these mesonic states with respect to the lowest Matsubara frequency are introduced [18]. Recently, studying QGP in presence of external magnetic field has been reported [19]. Also, the thermodynamics and higher-order moments with gluonic quasiparticles have been calculated from  $SU(3)$  PLSM [20].

The transport coefficients, which cannot be measured directly, are conjectured to characterize various essential properties of the system of interest, such as electric and heat conductivity and bulk and shear viscosity. It is obvious that the hydrodynamic models could play an essential role towards this goal. But in very limited cases, the QCD transport coefficients can be determined by means of numerical and even analytical methods [21–23]. The confrontation to the LQCD results enables the judgement about the effective models, such as PNJL and PLSM. The transport coefficients calculated from PNJL [24] and DQPM [25] and the thermodynamics and the bulk viscosity near phase transition from  $\mathcal{Z}(1)$  and  $\mathcal{O}(4)$  models in Hartree approximation for Cornwall–Jackiw–Tomboulis (CJT) formalism are summarized in [26]. The shear and bulk viscosities of the partonic and the hadronic matter from the parton-hadron-string dynamics (PHSD) were presented in [27]. The ratio of bulk and shear viscosity to the electric conductivity of QGP has been reported in [28].

In the present work, we introduce a calculation procedure that allows combining some transport coefficients to the relativistic hydrodynamics in an indirect way. We make benefit from the exact knowledge we have so far about the fundamental thermodynamic quantities such as the equation of state, specific heat, squared speed of sound and quark number multiplicity as a function of temperature at fixed chemical potential in order to determine electric and heat conductivity and bulk and shear viscosity. Doing this, we can estimate the relationship between these quantities and the possible experimental observations.

The present work is organized as follows. The PLSM approach shall be elaborated in Sec. II. Section III summarizes the chiral phase-structure from the PLSM and compares the phase transition for light and strange quarks with LQCD calculations. The estimation of the decay widths and the relaxation time of quarks and gluons is given in Sec. III B. The thermodynamic quantities, which are conjectured to play an essential role in estimating the transport coefficients such as, trace anomaly, specific heat, squared speed of sound, the quark number multiplicity and the quark number susceptibility as a function of  $T$  at different chemical potentials will be calculated in Sec. III C. The normalized electric and heat conductivities are outlined in Sec. III D 1. The ratios of bulk and shear viscosities relative to the thermal entropy density are given in Sec. III D 2. Also, the different scenarios for the ratios of conductivities and the different types of viscosity are specified in this section. Section IV is devoted to conclusion and outlines.

## II. REMINDER OF THE QCD-LIKE APPROACH

**A.  $SU(3)$  Polyakov Linear- $\sigma$  Model.** The PLSM Lagrangian with  $N_f = 3$  quark flavors and  $N_c = 3$  color degrees of freedom consists of two parts

$$\mathcal{L} = \mathcal{L}_{\text{chiral}} - \mathcal{U}(\phi, \phi^*, T). \quad (1)$$

The chiral part  $\mathcal{L}_{\text{chiral}} = \mathcal{L}_q + \mathcal{L}_m$ , which is coupled to the Polyakov loop potential with  $SU(3)_L \times SU(3)_R$  symmetry [16, 29], consists, in turn, of two potential types, the first one tends to the fermionic contribution of quarks, Eq. (2), coupled with a flavor-blind Yukawa coupling  $g$  of the quarks [30], i. e., the quarks are coupled to the mesons

$$\mathcal{L}_q = \sum_f \bar{q}_f (i\gamma^\mu D_\mu - gT_a(\sigma_a + i\gamma_5\pi_a))q. \quad (2)$$

The second one refers to the mesonic contribution, Eq. (3),

$$\begin{aligned} \mathcal{L}_m = & \text{Tr} (\partial_\mu \Phi^\dagger \partial^\mu \Phi - m^2 \Phi^\dagger \Phi) - \lambda_1 [\text{Tr} (\Phi^\dagger \Phi)]^2 - \\ & - \lambda_2 \text{Tr} (\Phi^\dagger \Phi)^2 + c [\text{Det} (\Phi) + \text{Det} (\Phi^\dagger)] + \text{Tr} [H(\Phi + \Phi^\dagger)]. \end{aligned} \quad (3)$$

Through the covariant derivative  $D_\mu = \partial_\mu - iA_\mu$ , the quarks can be coupled to the Euclidean gauge field [31, 32]  $A_\mu \simeq \delta_{\mu 0} A_0$ . In Eq. (3),  $\Phi$  is a complex  $3 \times 3$  matrix depending on  $\sigma_a$  (scalar fields) and  $\pi_a$  (pseudoscalar fields) [16],  $\Phi = T_a \phi_a = T_a(\sigma_a + i\pi_a)$ , where  $T_a = \lambda_a/2$  with  $a = 0, \dots, 8$  are the nine generators of the  $U(3)$  symmetry group and  $\lambda_a$  are the eight Gell-Mann matrices [33],  $\gamma^\mu$  are the chiral spinors,  $\sigma_a$  are the scalar mesons, and  $\pi_a$  are the pseudoscalar mesons.

The chiral symmetry is explicitly broken by  $H$  which is a  $3 \times 3$  matrix with nine parameters  $h_a$ ,  $H = T_a h_a$ . Exact three finite condensates  $\bar{\sigma}_0$ ,  $\bar{\sigma}_3$ , and  $\bar{\sigma}_8$  are likely, because the finite vacuum expectation values of  $\Phi$  and  $\bar{\Phi}$  are conjectured to carry the quantum numbers of vacuum, and the diagonal components of the explicit symmetry breaking term  $h_0$ ,  $h_3$ , and  $h_8$  should not vanish [34]. Therefore, the parameters  $h_a$ , with  $h_0 \neq 0$ ,  $h_3 = 0$  and  $h_8 \neq 0$ , and the squared tree-level mass of the mesonic fields  $m^2$ , two possible coupling constants  $\lambda_1$  and  $\lambda_2$ , Yukawa coupling  $g$ , and a cubic coupling constant  $c$  can be estimated  $c = 4807.84 \text{ MeV}$ ,  $h_1 = (120.73)^3 \text{ MeV}^3$ ,  $h_s = (336.41)^3 \text{ MeV}^3$ ,  $m^2 = -(306.26)^2 \text{ MeV}^2$ ,  $\lambda_1 = 13.48$  and  $\lambda_3 = 46.48$  and  $g = 6.5$ .

In presence of  $U(1)_A$  axial anomaly of the QCD vacuum, it is convenient to convert the condensates  $\sigma_0$  and  $\sigma_8$  into a light and strange quark condensate,  $\sigma_l$  and  $\sigma_s$ , based on an orthogonal basis transformation [35]

$$\begin{pmatrix} \sigma_l \\ \sigma_s \end{pmatrix} = \frac{1}{\sqrt{3}} \begin{pmatrix} \sqrt{2} & 1 \\ 1 & -\sqrt{2} \end{pmatrix} \begin{pmatrix} \sigma_0 \\ \sigma_8 \end{pmatrix}. \quad (4)$$

The Polyakov-loop effective potential [31] which is given in the second term of Eq. (1),  $\mathcal{U}(\phi, \phi^*, T)$ , introduces dynamics to the expectation value of the color traced Wilson loop in the temporal direction  $\phi(\vec{x}) = \langle \mathcal{P}(\vec{x}) \rangle / N_c$  so that  $\phi = (\text{Tr}_c \mathcal{P}) / N_c$  and  $\phi^* = (\text{Tr}_c \mathcal{P}^\dagger) / N_c$ , where the Polyakov loop  $\mathcal{P}$  is inversely proportional to the color degree of freedom  $N_c$  [31],

$$\mathcal{P}(\vec{x}) = \mathcal{P} \exp \left[ i \int_0^{1/T} d\tau A_4(\vec{x}, \tau) \right], \quad (5)$$

where  $A_4 = iA^0$  is called Polyakov gauge [31,32]. It was found that enlarging  $N_c$  decreases the critical temperature of the deconfinement phase transition [18].

For the temperature dependence of the Polyakov loop in pure Young–Mills theory, we utilize a temperature-dependent potential  $U(\phi, \phi^*, T)$  having  $Z(3)$  center symmetry as that of the pure gauge QCD Lagrangian [6, 8]. The Polyakov loops  $\phi$  and  $\phi^*$  are considered as order parameter for the deconfinement phase-transition [6, 8]. In the present work,  $U(\phi, \phi^*, T)$  is given as a polynomial expansion in  $\phi$  and  $\phi^*$  [5, 6, 8, 36],

$$\frac{\mathcal{U}_{\text{poly}}(\phi, \phi^*, T)}{T^4} = -\frac{b_2(T)}{2}(|\phi|^2 + |\phi^*|^2) - \frac{b_3}{6}(\phi^3 + \phi^{*3}) + \frac{b_4}{16}(|\phi|^2 + |\phi^*|^2)^2, \quad (6)$$

where  $b_2(T) = a_0 + a_1(T_0/T) + a_2(T_0/T)^2 + a_3(T_0/T)^3$ . The parameters  $a_0 = 6.75$ ,  $a_1 = -1.95$ ,  $a_2 = 2.625$ ,  $a_3 = -7.44$ ,  $b_3 = 0.75$ , and  $b_4 = 7.5$  reproduce the pure gluonic QCD thermodynamics and describe the Polyakov loop as a function of temperature. For a better agreement with LQCD results, the critical temperature  $T_0$  is fixed at 270 MeV, especially in the pure gauge sector.

**B. Mean Field Approximation.** In thermal equilibrium and by using a path integral over the quark, antiquark, and meson field, the grand partition function can be defined as

$$\mathcal{Z} = \int \prod_a \mathcal{D}\sigma_a \mathcal{D}\pi_a \int \mathcal{D}\psi \mathcal{D}\bar{\psi} \exp \left[ \int_x \left( \mathcal{L} + \sum_{f=u,d,s} \mu_f \bar{\psi}_f \gamma^0 \psi_f \right) \right], \quad (7)$$

where  $\int_x \equiv i \int_0^{1/T} dt \int_V d^3x$  with  $V$  being the volume of the system, and  $\mu_f$  is the chemical potential for quark flavors  $f = (u, d, s)$ . We assume symmetric quark matter and degenerate light quarks and therefore define a uniform flavor blind chemical potential  $\mu_f \equiv \mu_{u,d} = \mu_s$  [7, 16, 30].

For the meson fields, their expectation values  $\bar{\sigma}_l$  and  $\bar{\sigma}_s$  can be estimated by means of mean field approximation [14, 37]. Standard methods [37] are used in calculating the integrals over the fermions yields. Then, the thermodynamic potential density  $\Omega(T, \mu) = -T \ln \mathcal{Z}/V$  is

$$\Omega(T, \mu) = U(\sigma_l, \sigma_s) + \mathcal{U}(\phi, \phi^*, T) + \Omega_{\bar{\psi}\psi}. \quad (8)$$

The quark and antiquark potential has been introduced in [14, 37]

$$\begin{aligned} \Omega_{\bar{\psi}\psi} = & -2TN_f \int_0^\infty \frac{d^3\vec{p}}{(2\pi)^3} \times \\ & \times \left\{ \ln \left[ 1 + 3(\phi + \phi^* e^{-(E-\mu)/T}) \times e^{-(E-\mu)/T} + e^{-3(E-\mu)/T} \right] + \right. \\ & \left. + \ln \left[ 1 + 3(\phi^* + \phi e^{-(E+\mu)/T}) \times e^{-(E+\mu)/T} + e^{-3(E+\mu)/T} \right] \right\}, \quad (9) \end{aligned}$$

where  $N_f$  gives the number of the quark flavors,  $E = \sqrt{\vec{p}^2 + m^2}$  is the energy of the valence quark and antiquark, for both light and strange quarks [35], where  $m_l = g\sigma_l/2$  and  $m_s = g\sigma_s/\sqrt{2}$ .

The purely mesonic potential is given as

$$U(\sigma_l, \sigma_s) = -h_l\sigma_l - h_s\sigma_s + \frac{m^2(\sigma_l^2 + \sigma_s^2)}{2} - \frac{c\sigma_l^2\sigma_s}{2\sqrt{2}} + \frac{\lambda_1\sigma_l^2\sigma_s^2}{2} + \frac{(2\lambda_1 + \lambda_2)\sigma_l^4}{8} + \frac{(\lambda_1 + \lambda_2)\sigma_s^4}{4}. \quad (10)$$

Equations (6), (9), and (10) construct the thermodynamic potential density, Eq. (8), in which seven parameters  $m^2, h_l, h_s, \lambda_1, \lambda_2, c,$  and  $g$ , condensates  $\sigma_l$  and  $\sigma_s$ , and order parameters for the deconfinement  $\phi$  and  $\phi^*$  should be determined. First, the six parameters  $m^2, h_l, h_s, \lambda_1, \lambda_2$  and  $c$  can be fixed in vacuum by six experimentally known quantities [16]. In order to evaluate  $\sigma_l, \sigma_s, \phi,$  and  $\phi^*$ , the thermodynamic potential, Eq. (8), should be minimized with respect to  $\sigma_l, \sigma_s, \phi,$  and  $\phi^*$

$$\left. \frac{\partial\Omega}{\partial\sigma_l} = \frac{\partial\Omega}{\partial\sigma_s} = \frac{\partial\Omega}{\partial\phi} = \frac{\partial\Omega}{\partial\phi^*} \right|_{\min} = 0, \quad (11)$$

meaning that  $\sigma_l = \bar{\sigma}_l, \sigma_s = \bar{\sigma}_s, \phi = \bar{\phi},$  and  $\phi^* = \bar{\phi}^*$ , especially at vanishing chemical potential, are the global minimum.

### III. RESULTS

In order to calculate the transport coefficients, other quantities, including the phase transition, the quark decay constant and the quark number susceptibility, should be estimated first.

**A. Phase Transitions and Their Order Parameters.** The fundamental thermodynamical quantities can be deduced from the partition function  $\mathcal{Z}$ , Eq. (8). When the thermodynamical potential, Eq. (8), should be globally minimized,  $\sigma_l, \sigma_s, \phi,$  and  $\phi^*$  can be determined. In vacuum,  $\sigma_{l_0} = 92.4$  MeV and  $\sigma_{s_0} = 94.5$  MeV, respectively [14, 16].

In the left-hand panel of Fig. 1, the normalized chiral condensates,  $\sigma_l/\sigma_{l_0}$  and  $\sigma_s/\sigma_{s_0}$ , which correspond to the light and strange quarks, respectively, are given as a function of temperature. The normalization is calculated with respect to  $\sigma_{l_0}$  and  $\sigma_{s_0}$ , respectively. At vanishing chemical potential, the two Polyakov-loop potentials (characterizing deconfinement phase-transition) are identical, i. e.,  $\langle\phi\rangle = \langle\phi^*\rangle$ . The right-panel shows the temperature dependence of the quark-number susceptibilities of the chiral and that of the deconfinement phase-transitions. The quark-number susceptibility is deduced from the temperature derivative of the corresponding quantity. It is apparent that the quark-number susceptibilities can be estimated directly from the thermodynamical potential, Eq. (8).

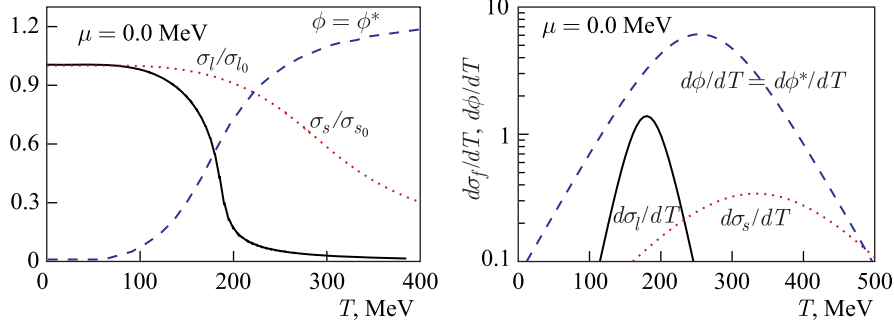


Fig. 1 (color online). Left-hand panel: the normalized chiral condensates  $\sigma_l$  and  $\sigma_s$  (solid and dotted curves, respectively) and the Polyakov loop potential, the order parameters  $\phi$  and  $\phi^*$  (dashed curve) are given as a function of temperature at vanishing baryon chemical potential. The right-hand panel shows the temperature dependence of the chiral susceptibilities for light and strange quarks (solid and dotted curves, respectively) and that for the deconfinement phase-transition (dashed curve)

In order to estimate the critical temperature, two approaches can be implemented:

- the intersect of the order parameter with the corresponding chiral condensate, the left-hand panel of Fig. 1.
- the peak in the thermal evolution of the strange and nonstrange chiral condensates, the right-hand panel of Fig. 1.

In this way and according to the right-hand panel of Fig. 1, we can estimate the chiral restoration temperatures. The critical temperature from the light quark-number susceptibility obviously differs from the strange quark-number susceptibility. The broken chiral-symmetry for the light condensate is restored at  $T_\chi^l \sim 181$  MeV. For strange quark the restoration comes off at  $T_\chi^s \sim 220$  MeV. The critical temperature of the deconfinement phase-transition seems to have a higher value,  $T_c^d \sim 256$  MeV.

Furthermore, the PLSM can be exploited to determine the physical masses of the degenerated light and strange quarks under the assumption that the quark chemical potentials are equivalent,  $\mu_u = \mu_d = \mu_s$ . It is worthwhile to devote further efforts to determining the correlations and the fluctuations between the chiral and deconfinement phase-transition(s). According to the direct dependence of quark masses on their condensates,  $m_l = g\sigma_l/2$  and  $m_s = g\sigma_s/\sqrt{2}$ , and when taking into account the flavor-blind Yukawa coupling  $g = 6.5$ , one can straightforwardly deduce that the mass of the light constituent quark  $m_l \sim 300$  MeV and that of the strange constituent quark  $m_s \sim 433$  MeV. In deducing chiral condensates, various approaches have been implemented:

- From the combined light and strange condensates as calculation in lattice, the subtracted condensate is given as [38]

$$\Delta_{l,s} = \frac{\langle \bar{l}l \rangle - \left( \frac{m_l}{m_s} \right) \langle \bar{s}s \rangle \Big|_T}{\langle \bar{l}l \rangle - \left( \frac{m_l}{m_s} \right) \langle \bar{s}s \rangle \Big|_{T=0}}, \quad (12)$$

which obviously reads the ratio of the net light to strange quark condensates at finite temperature  $T$  to that at vanishing temperature [39]. This requires estimating the quark-masses dependence on the chiral condensate at vanishing and finite temperature.

- From PLSM with  $2 + 1$  quark flavors [40], it was found that the subtracted condensate is related to the fit parameters but with three degenerate quark flavors. In this case, replacing  $m_l$  and  $m_s$  by  $h_l$  and  $h_s$ , respectively, leads to

$$\Delta_{l,s} = \frac{\sigma_l - \left( \frac{h_l}{h_s} \right) \sigma_s \Big|_T}{\sigma_l - \left( \frac{h_l}{h_s} \right) \sigma_s \Big|_{T=0}}. \quad (13)$$

- From lattice QCD simulations, the dimensionless quantities are preferable. Thus, the chiral order-parameter can be expressed in terms of the chiral condensate [41],

$$M_b = \frac{m_s \langle \bar{\sigma}_l(T, \mu) \rangle}{T^4}. \quad (14)$$

The left-hand panel of Fig.2 presents the subtracted chiral condensates as a function of temperature at vanishing baryon chemical potential. The PLSM calculations are compared with various  $2 + 1$  lattice QCD simulations, in which asqtad [43] and p4 [44,45] improved staggered fermion actions with almost physical strange and light quark masses and temporal extent  $N_\tau = 8$  are implemented. The agreement between both sets of calculations is excellent. The steeper drop in the chiral subtracted condensate comes from the pure gluonic potential in the grand canonical calculation in absence of the gluons interaction. The latter should be improved with the inclusion of Polyakov loop potential.

It is evident that  $\Delta_{l,s}$  remains finite at low  $T$ . Near  $T_c$ ,  $\Delta_{l,s}$  decreases very rapidly within a narrow range of temperatures, i.e., the light quark and gluon degrees of freedom liberate, and the deconfinement and/or the restoration of broken chiral symmetry take place. It is worthwhile to highlight that the introducing of the Polyakov loop corrections improves the calculation of the pure gluonic potential through a gluon contribution, which causes smoothing chiral-transition or repaid crossover [39,42].

The right-hand panel shows the temperature dependence of  $M_b$ , which combines the strange quark mass with the light condensate normalized over  $T^4$ . The

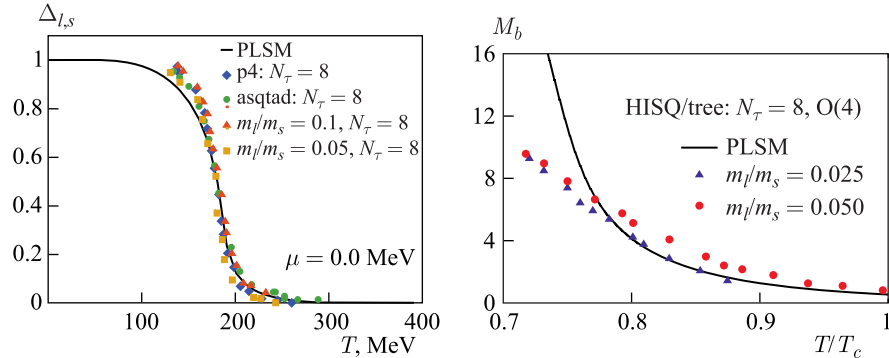


Fig. 2 (color online). Left-hand panel: the subtracted condensate given as a function of temperature at vanishing baryon chemical potential is compared with the lattice QCD results [39, 42]. Right-hand panel: the order parameter,  $M_b$ , Eq.(14), calculated from PLSM (solid curve) is compared with lattice QCD simulations implementing HISQ/tree action [41],  $N_\tau = 8$ ,  $M_q/M_s = 0.025$  (triangles) and  $M_q/M_s = 0.05$  (circles)

PLSM calculations (solid curve) are compared with HISQ/tree lattice QCD with  $N_\tau = 8$  and two values for the quark masses,  $M_q/M_s = 0.025$  (triangles) and  $M_q/M_s = 0.05$  (circles) [41]. The agreement between the two sets of calculations is convincing, especially at high temperatures.

**B. Dynamics of Gluonic Quasiparticles.** The dynamical quasiparticle model (DQPM) describes the phenomenology of interacting massless quarks and gluons as noninteracting *massive* quasiparticles [46–48]. The gluonic and quark decay widths and the relaxation time for quarks and gluons can be determined [48]. It was found that DQPM describes well the QCD properties in terms of single-particle Green’s function, especially above the critical temperatures [48]. The model parameters are fitted in order to construct the equation of state at high temperatures [48].

In DQPM, the coupling constant  $g^2$  (squared) at  $T > T_c$  has been approximated as [48]

$$g^2(T/T_c) = \frac{48\pi^2}{(11N_c - 2N_f) \ln[\lambda^2(T/T_c - T_s/T_c)^2]}, \quad (15)$$

where  $\lambda = 2.42$  and  $T_s = 0.56 T_c$  are parameters extracted from the fit to the lattice QCD results with  $N_f = 0$  [48]. Alternatively, a slightly different analytical form for  $g^2(T/T_c)$ , which was fitted with the lattice QCD data [49], can also be implemented. Accordingly, it was found that the effective gluons and

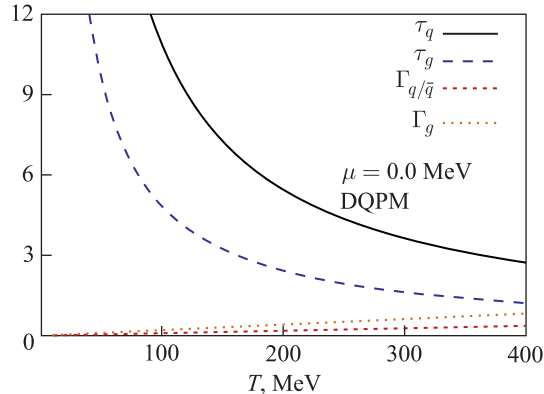


Fig. 3 (color online). The temperature dependence of the decay constants of quarks, antiquarks and gluons (long dotted and dotted curves) and their relaxation times (solid and dashed curves) at vanishing chemical potential are calculated from the dynamical quasiparticle model

quarks and antiquarks, respectively, have finite decay widths at vanishing baryon chemical potential [48]

$$\Gamma_g(T) = \frac{1}{3} N_c \frac{g^2 T}{8\pi} \ln \left( \frac{2c}{g^2} + 1 \right), \quad (16)$$

$$\Gamma_{q(\bar{q})}(T) = \frac{1}{3} \frac{N_c^2 - 1}{2N_c} \frac{g^2 T}{8\pi} \ln \left( \frac{2c}{g^2} + 1 \right), \quad (17)$$

where the parameter  $c = 14.4$  is related to a magnetic cutoff [48]. In frame of DQPM, the flavor blind reaction rates for quarks and gluons are inversely-dependent on the decay width,  $\tau_q \sim 1/\Gamma_q$  and  $\tau_g \sim 1/\Gamma_g$ , respectively. These two quantities are essential in computing the electrical and the thermal conductivity, Sec. III D.

Also for bulk and shear viscosity, the relaxation time plays an important role. Figure 3 presents the dependence of the quark and gluon relaxation time and their decay widths on the temperature at vanishing baryon chemical potential as calculated from DQPM. From Eqs. (16) and (17), the relaxation time is approximately inversely proportional to the decay width. We notice that the thermal evolution of the quark relaxation time is shorter than that of the gluon, while the values of gluonic decays widths are smaller than those of the quarks.

**C. Thermodynamics.** The thermodynamical quantities can be estimated from the free energy density of the canonical partition function  $\mathcal{Z}$  at vanishing baryon chemical potential. In the present work, we want to introduce the thermodynamical quantities needed in computing conductivities and viscosities, such as the interaction measure, speed of sound  $c_s^2$ , specific heat  $c_V$  and higher-orders of the quark number multiplicity.

1. *Interaction Measure.* The normalized interaction measure can be derived from trace of the energy-momentum tensor,  $T_\nu^\mu = \epsilon - 3p$ ,

$$\frac{\Delta}{T^4} = \frac{\epsilon - 3p}{T^4}, \quad (18)$$

with  $\epsilon(p)$  being the energy density (pressure). Therefore, the normalized interaction measure can be related to the QCD running strong coupling constant,  $\propto T^4 \alpha_s^2$  [50].

In Fig. 4, the temperature dependence of the normalized interaction measure  $\Delta/T^4$ , Eq. (18), from LSM with the quark flavor blind Yukawa coupling constant  $g = 6.5$  and from PLSM with  $g = 6.5$  and  $10.5$  is illustrated. The results are compared with different lattice QCD calculations with asqtad [43] and p4 actions [44,45], temporal number  $N_\tau = 8$  as well as in the continuum extrapolated limit [42].

We notice that the thermal dependence of the normalized interaction measure, which is estimated at Yukawa coupling  $g = 6.5$ , describes well the lattice QCD calculations with asqtad action and  $N_\tau = 8$  (square points) [51]. When increasing the Yukawa coupling to  $10.5$ , the peak gets closer to the lattice QCD calculations with p4 action and  $N_\tau = 8$  (triangle points) [42]. In the hadron phase, the in-

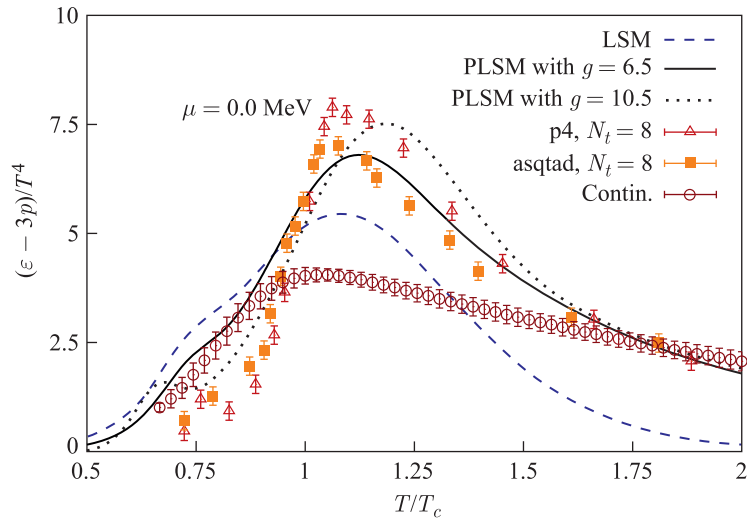


Fig. 4 (color online). The trace anomaly  $(\epsilon - 3p)/T^4$  as a function of temperature at vanishing baryon chemical potential is calculated from LSM (dashed curve) and PLSM with Yukawa coupling constants  $g = 6.5$  (solid curve) and  $g = 10.5$  (dotted curve) and compared with lattice QCD calculations (triangle, square and circle symbols) [42], [51]

teraction measure is small and increases with the temperature. A peak appears at the critical temperature. Further increase in the temperature decreases the interaction measure, i. e., derives the system stronger in the deconfinement status. The critical temperature in lattice calculations  $T_c \sim 181 \pm 9$  MeV. Inserting Polyakov loop potential in LSM moves the peak to a higher temperature. Accordingly,  $T_\chi \sim 240$  MeV (in PLSM).

2. *Speed of Sound and Specific Heat.* Analogously to hydrodynamical approaches, which have been applied on the relativistic heavy-ion collisions and conducted the RHIC discovery of 2004, the speed of sound  $c_s$  is also an essential

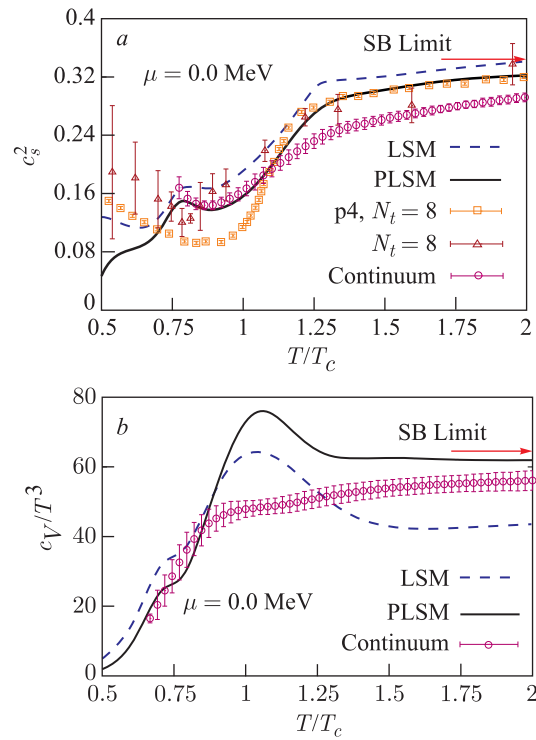


Fig. 5 (color online). *a*) The speed of sound squared calculated as a function of temperature at vanishing baryon chemical potential from LSM (dashed curve) and PLSM (solid curve) is compared with the lattice QCD calculations [52] (triangle points), [42] (square points) and [51] (circle points). *b*) The temperature dependence of the dimensionless specific heat  $c_V/T^3$  is calculated from LSM (dashed curve) and PLSM (solid curve) at vanishing baryon chemical potential and compared with the lattice QCD results [51]. In both panels, the arrow in upper right corner refers to the Stefan–Boltzmann-limit

quantity to be estimated. The speed of sound is related to the equation of state  $p(\epsilon)$ . At a constant entropy

$$c_s^2 = \left( \frac{\partial p}{\partial \epsilon} \right)_s = \frac{s}{c_v}, \quad (19)$$

where the specific heat  $c_v$  gives the thermal rate change of the energy density at a constant volume,

$$c_v = \left( \frac{\partial \epsilon}{\partial T} \right)_v. \quad (20)$$

In Fig. 5, the temperature dependence of the speed of sound squared (left-panel) and the specific heat at a constant volume (right-panel) are calculated at vanishing baryon chemical potential. In the left-hand panel, the results from LSM and PLSM are compared with lattice QCD calculations [42] (square points) with  $N_\tau = 8$  and [51] (square points) in the continuum limit extrapolation. A satisfying agreement between lattice QCD and PLSM is obtained, especially above the critical temperature  $T_c$ . The temperature is normalized with respect to  $T_c$ , where the lattice  $T_c \sim 181 \pm 9$  MeV, while the chiral restoration temperature from PLSM  $T_\chi \sim 240$  MeV. It is obvious that the speed of sound  $c_s^2$  approaches the Stefan–Boltzmann limit,  $1/3$ , at very high temperatures. The peak, which appears near the critical temperature, is due to the fast rate of the energy density change with increasing temperature. The temperature dependence of the specific heat calculated from LSM and PLSM at vanishing baryon chemical potential is presented in the right-hand panel of Fig. 5. The presence of color and gluon interactions, which are included through the Polyakov loop potential, tends to enhance the peak.

*3. Higher-Order of Quark Number Multiplicity.* In this section, we introduce the first two higher-order moments, which refer to the particle number multiplicity distribution and susceptibility calculated from PLSM. Studying the dependence of quark number on the temperature is equivalent to analysis of the thermal evolution of the fluctuations in the degrees of freedom of the system, which has a net-number of light or strange quarks. Here, we assume degenerate quarks so that the baryon chemical potentials  $\mu_u = \mu_d = \mu_s$ . The second-order moment,  $\chi_q$ , stands for the variance in the given distribution, i. e., how far a set of numbers spread out  $\delta n_q = n_q - \langle n_q \rangle$ . The dimensionless quark-number and quark number susceptibility can be deduced as

$$\frac{n_q(T, \mu)}{T^3} = -\frac{\partial \Omega(T, \mu)}{T^3 \partial \mu}, \quad (21)$$

$$\frac{\chi_q(T, \mu)}{T^2} = -\frac{\partial^2 \Omega(T, \mu)}{T^2 \partial \mu^2}. \quad (22)$$

The temperature dependence of dimensionless quantities, quark number (left-hand) and quark-number susceptibility (right-hand panel) at different baryon

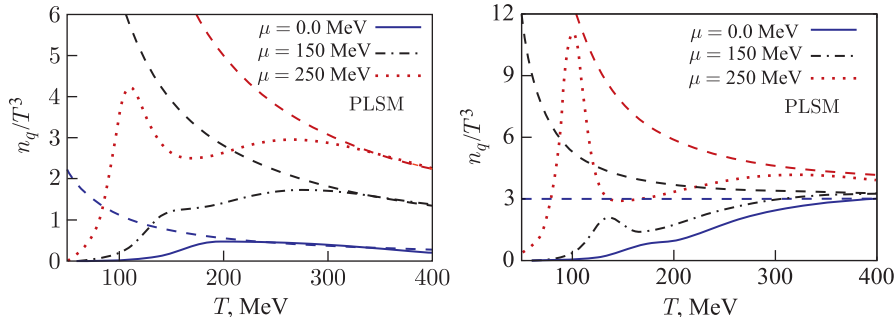


Fig. 6 (color online). Left-hand panel: the temperature dependence of the dimensionless quark number density  $n_q/T^3$  calculated from PLSM at different baryon chemical potentials,  $\mu = 0$  (solid), 150 (dot-dashed), and 250 MeV (dotted curve) is compared with the Stefan–Boltzmann limits (dashed curves diverging at low  $T$ ) at the same values of  $\mu$ . Right-hand panel: the same as in the left-hand panel but for the dimensionless quark number susceptibility,  $\chi_q/T^2$

chemical potential  $\mu = 0, 150$  and  $250$  MeV is shown in Fig. 6. Both quantities are compared with the thermal dependence of the Stefan-Boltzmann limits at the same values of the baryon chemical potential. It is conjectured that this comparison reflects the change in the number of quarks and antiquarks leaving/entering the system of interest. Increasing chemical potential seems to reduce the idealization of the system with massless gluonic or fermions, i. e., brings the system closer to the Stefan–Boltzmann limits. Furthermore, it is obvious that increasing  $\mu$  increases both  $n_q(T, \mu)/T^3$  and  $\chi_q(T, \mu)/T^2$  and enhances the peaks in both quantities. The quark-number susceptibility corresponding to large  $\mu$  approaches idealization with massless gluonic or fermions faster than the one at smaller  $\mu$ .

**D. Transport Coefficients.** QGP properties represent theoretical, experimental and even numerical challenge. In high-energy experiments, detectors are designed to register hadron-, lepton-, and electromagnetic signals. Partons are not detectable, at least directly. This explains why the properties of QGP are still not tackled, experimentally. Nonperturbative QCD is very sophisticated. Furthermore, lattice QCD at finite baryon chemical potential suffers from the so-called sign-problem, which breaks down the MC computational techniques. Effective models, such as LSM and NJL, in which some QCD dof, symmetries, dynamics, etc., are included, play an essential role. In the present work, we discuss main lines in determining the transport coefficients including conductivities and viscous properties of QGP. We compare the PLSM results with the available results of lattice QCD simulations.

*1. Electric and Heat Conductivity.* Due to deconfinement of color charges, one may expect that QGP is a quite good conductor [28]. We shall see that this

guess is related to the electrical but to the thermal conductivity. The electrical conductivity  $\sigma_e$  is a key transport coefficient, which recently gains an increasing interest among particle physicists. This physical property is related to the flow of the charge carriers, especially in presence of an electric field and can be measured by various methods. The first one applies an empirical methodology, where an external electric field is applied on the system of interest. The induced electric current  $\vec{j} = \sigma_e \vec{E}$ , with  $\sigma_e$  being the proportionally constant, can be evaluated [28]. The second one refers the self-interaction between quarks and gluons, i. e., no external electric field is needed. This is known as Green–Kubo corrector [28, 53, 54].

Analogously to classical gasses, i. e., Durde–Lorentz conductivity [53],

$$\sigma_e(T, \mu) = \sum_k \frac{4\pi}{137} q_k^2 \frac{n_k(T, \mu) \tau_k(T, \mu)}{m_k(T, \mu)}, \quad (23)$$

where  $k$  runs over quarks  $u, d, s$ , and antiquarks  $\bar{u}, \bar{d}, \bar{s}$ , and gluons  $g$ , while  $q$  are their electric charges, the electric conductivity of QCD can be estimated [54]. Accordingly, the functions  $n_k$ ,  $\tau_k$ , and  $m_k$ , which stand for number density, relaxation time and mass in dependence on  $T$  and  $\mu$ , respectively, are to be directly implemented in the strong interaction system. The factor  $4\pi/137$  counts the electromagnetic fine structure constant and the summation over fractional electric charges.

The heat conductivity  $\kappa(T, \mu)$  is related to the heat flow in the relativistic fluid [55–58] and gives an indicator about the rate of the energy change taking place in the system of interest. A simple way to estimate the evolution of heat conductivity is simulating the likely irradiation occurring in the system of interest by means of energetic ions [59]. From specific heat  $c_v$  and relaxation time  $\tau$ , the heat conductivity reads [60]

$$\kappa(T, \mu) = \frac{1}{3} \nu_{\text{rel}} c_V(T, \mu) \sum_k \tau_k(T, \mu), \quad (24)$$

where  $\nu_{\text{rel}}$  are the relative velocities. For simplicity, it was assumed that  $\nu_{\text{rel}} \sim 1$ . For two quarks with masses  $m_1$  and  $m_2$ , the center-of-mass collisions result in relative velocity  $\nu_{\text{rel}} = \sqrt{(p_1 p_2)^2 - (m_1 m_2)^2} / E_1 E_2$  [61]. In the relativistic limit, the quark masses are negligibly small relative to the momentum, where the quark masses decrease with increasing  $T$  according to the chiral condensate, Fig. 1, while the mean momentum increases remarkably,  $\nu_{\text{rel}} \sim 1$ .

The left-hand panel of Fig. 7 shows the temperature dependence of the electric conductivity  $\sigma_e/T$  at vanishing baryon chemical potential. The PLSM calculations are compared with various lattice results [62–65] and with some QCD-like effective models such as PHSD [27], NJL and DQPM [24].

The electric conductivity, which effectively depends on the temperature and the chemical potential, Eq. (23) is strongly related to the decay constant or the

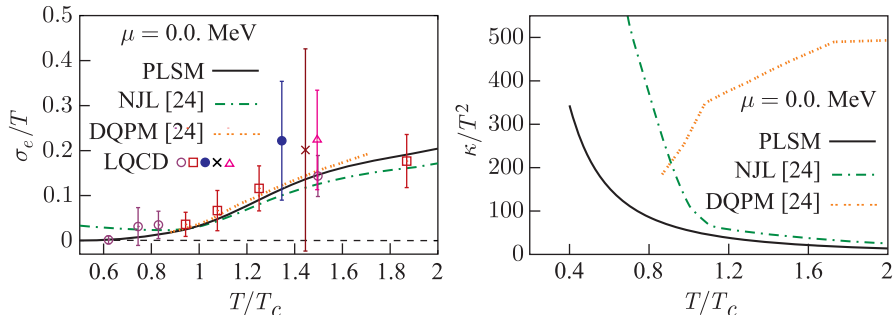


Fig. 7 (color online). Left-hand panel: electric conductivity given as a function of temperature at vanishing baryon chemical potential is calculated from PLSM (solid curve) and compared with the NJL [24] (dotted dash) and DQPM [24] (double dotted) and lattice QCD simulations [63] (circle points, square points), [65] (closed circle points), [64] (cross point) and [81] (open triangle). Right-hand panel: the heat conductivity normalized to  $T^2$  is calculated as a function of temperature at vanishing baryon chemical potential from PLSM (solid curve) and compared with NJL [24] (dotted dash) and DQPM (double dotted) [24]

relaxation time of the quarks. Because of the interaction between quarks and gluons, the increase in the baryon chemical potential increases the quark and antiquark numbers, (see the left-hand panel of Fig. 6). The PLSM results of the dimensionless quantity  $\sigma_e/T$  are compared with different QCD-like models, NJL and DQPM [24] and lattice QCD simulations [63], where the circles denote the lattice size  $N_s = 24^3$ , and the square symbols represent calculation on  $N_s = 32^3$  lattice. In both calculations 2 + 1 quark obtained number of flavors are used. Furthermore, the lattice QCD results given as closed circles [65] and crosses [64] are with finite quark flavors, while the open triangles are lattice QCD calculations [81] with out flavor.

In neutral units and in free space, the electric conductivity is multiplied by  $e^2 = 4\pi\alpha$  and quark electric charges  $\sum q_k$ , where the electromagnetic coupling or the fine-structure constant at zero energy  $\alpha = 1/137$  [63]. The lattice QCD simulations are normalized by the quark charges 5/9 for  $N_f = 2$  and electron charge  $e$  [63]. The PLSM results agree well with the lattice calculations [63], especially up to  $T > T_c$ . From the temperature dependence of the electric conductivity calculated from PLSM and compared with some other QCD-like models, such as NJL and DQPM [24], we conclude that the PLSM results are most comparable with the lattice QCD simulations [63]. The PLSM electric conductivity curve, which is calculated from Eq. (23), refers to a combination between the quark-number multiplicity and their masses. Despite the quark relaxation time was estimated from DQPM, the DQPM and NJL results [24] fairly agree with the lattice QCD [63], especially at  $T < T_c$ .

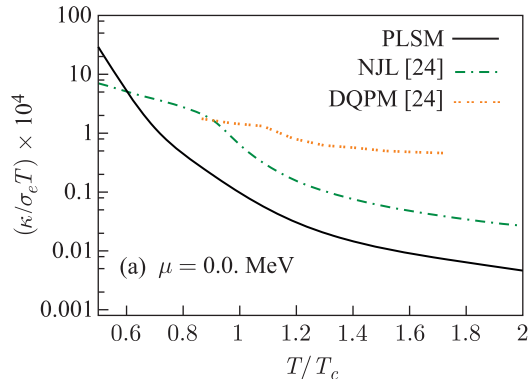


Fig. 8 (color online). The numerical estimation for the ratio of heat-to-electric conductivities as a function of temperature at vanishing baryon chemical potential is compared with PLSM (solid curve), NJL (dotted dash), and DQPM (double dotted) [24]

The right-hand panel of Fig. 7 shows the heat conductivity normalized to  $T^2$  as a function of temperature at vanishing baryon chemical potential. The PLSM calculations are compared with NJL and DQPM [24]. It is worthwhile to highlight that these different models have different critical temperatures,  $T_c \sim 240$  MeV from PLSM,  $T_c \sim 200$  MeV from NJL, and  $T_c \sim 158$  MeV from DQPM. The temperature dependence of NJL heat conductivity normalized to  $T^2$ , Eq. (24), decreases faster than the one from PLSM [24]. From DQPM, the temperature dependence is the opposite. Here, increasing temperature increases the heat conductivity. There are no lattice QCD calculations to compare with it.

Figure 8 presents the numerical estimation for the ratios  $\kappa/T^2$ -to- $\sigma_e/T$  calculated from different effective models. From PLSM, this ratio rapidly decreases. It is faster than the ones calculated from NJL and DQPM [24], especially at temperatures exceeding the critical one  $T_c$ . This no longer depends on the relaxation time. There are no lattice QCD calculations to be compared with. At  $T > T_c$ , the ratios from the different models are distinguishable by about one order of magnitude.

*2. Bulk and Shear Viscosity.* The discussion about the transport coefficients would not be entirely without the viscosity, which is strongly related to the hydrodynamical flow of the relativistic fluid, the hadron and parton phases in our case, and the transverse motion of the particles during the expansion of the strongly interacting system [66,67]. In other words, the estimation of viscosity is very essential to check out the evaluation of the physical observables such as the elliptic flow  $v_2$  [66,67] and the correlation functions [66,67].

Also, the viscosity is related to thermodynamical quantities such as trace anomaly, specific heat and speed of sound [68]. According to Kubos formula, the

bulk viscosity is related to the correlation functions of the trace of the energy-momentum tensor  $T_\mu^\nu$  [68],

$$\xi = \lim_{\omega \rightarrow 0} \frac{1}{9\omega} \int_0^\infty dt \int dr^3 \langle [T_\mu^\nu(x), T_\mu^\nu(0)] \rangle e^{i\omega t}, \quad (25)$$

where  $\omega$  is the frequency of quark and gluon vibration [68]. For a narrow frequency region,  $\omega \rightarrow \omega_0 \equiv \omega_0(T) \sim T$  [68]. Thus, the bulk viscosity reads

$$\xi = \frac{1}{9T} \left[ T^5 \frac{\partial}{\partial T} \left( \frac{\epsilon - 3p}{T^4} \right) + 16|\epsilon_v| \right] = \frac{1}{9T} [-16\epsilon + 9TS + Tc_V + 16|\epsilon_v|], \quad (26)$$

with  $\epsilon_v$  being the vacuum energy density, which is to be estimated from the lattice QCD calculations and related to the critical temperature [68].

From the expressions of the speed of sound and the bulk viscosity [72], a relation between bulk and shear viscosities and the speed of sound [72] can be deduced as

$$\eta \sim \frac{\xi}{-0.45(c_s^2 - \frac{1}{3})}. \quad (27)$$

Expression (27) results in a behavior similar to the one introduced in [73, 74],

$$\eta \sim \frac{\xi}{(c_s^2 - \frac{1}{3})^2}. \quad (28)$$

In the left-hand panel of Fig. 9, the temperature dependence of the ratio of bulk viscosity  $\xi$  on the thermal entropy  $s(T)$  at vanishing baryon chemical potential is presented. The ratio of shear viscosity to the thermal entropy  $\eta/s$  as a function of temperature at vanishing baryon chemical potential is given in the right-hand panel. At temperatures close to the critical one, the ratio  $\xi/s$  shows a good agreement with the lattice QCD results [68–71]. The agreement with LSM [14, 75], DQPM and NJL models [24] are good, as well. The entropy tends to vanish in order to decrease temperature.

The ratio  $\xi/s$  can be estimated from the energy density and trace anomaly, Eq. (26). Around  $T_c$ , the energy density has a sudden change. Accordingly,  $\xi/s$  rapidly decreases and a first-order phase-transition turns to be likely. The sharp increase in the bulk viscosity nears to the phase transition or induces instability in the hydrodynamic flow of the plasma. This is responsible for some RHIC observables [76]. Thus, investigating  $\xi/s$  would have great impact on experimental observables.

From PLSM, the shear viscosity is very strongly related to the behavior of the speed of sound and the bulk viscosity, Eq. (27). A good agreement with the lattice QCD calculations [68–71] and other effective models [24, 27] is observed. In particular, the lower values of the ratio shear viscosity over entropy refers to low QGP

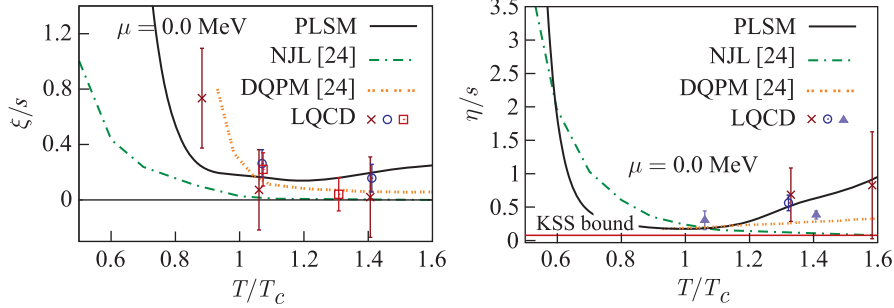


Fig. 9 (color online). Left-hand panel: the ratio of bulk viscosity and the thermal entropy  $\xi/s$  calculated from PLSM (solid curve) and compared with lattice QCD simulations [69] (cross points) and [70] (circle points and square points) is given as a function of temperature vanishing baryon chemical potential. The right-hand panel shows the ratio of shear viscosity to the thermal entropy  $\eta/s$  calculated from PLSM (solid curve) with the available lattice QCD simulations [69] (cross points), [70] (circle points and square points) and [71] (triangle points). The Kovtun–Son–Starinets (KSS) bound is shown. In both panels the results are compared with NJL (dotted dash) and DQPM (double dotted) [24]

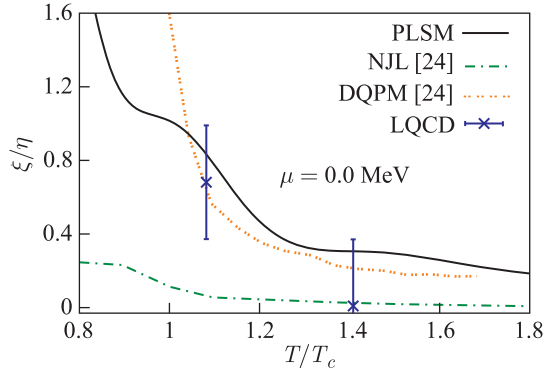


Fig. 10 (color online). The ratio of bulk to shear viscosities at vanishing baryon chemical potential is compared with lattice QCD results [69]

viscosity in the partonic phase [77]. This decrease is caused by the stronger interactions and released degrees of freedom. It is supported by the experimental description of the collective flow in heavy-ion collisions [78,79]. It is worthwhile to notice that the numerical estimation of the ratio of viscosity over thermal entropy from PLSM is higher than KSS bound [80]. The latter is  $T$ -independent,  $\sim 1/4\pi$ .

Figure 10 shows the ratio of bulk to shear viscosities as a function of temperature. When  $T$  approaches the critical value, a sudden drop takes place and the

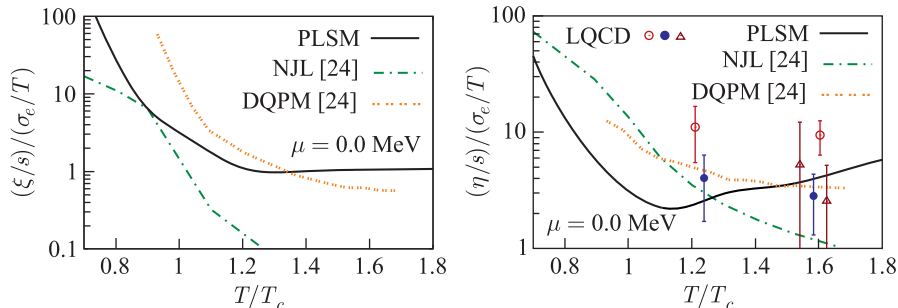


Fig. 11 (color online). In a log-scale, the thermal dependence of  $\xi/s$ -to- $\sigma_e/T$  (left-hand panel) and  $\eta/s$ -to- $\sigma_e/T$  (right-hand panel) is calculated as a function of temperature at vanishing baryon chemical potential from PLSM. In the left-hand panel, the results are confronted to the available results of lattice QCD simulations [81]

ratio tends to be  $T$ -independent. There is a maximum around the phase transition. This behavior is confirmed by the lattice QCD calculations [69].

In Fig. 11, the ratio of bulk and shear viscosities (normalized to the entropy) with the electric conductivities,  $(\xi/s)/(\sigma_e/T)$  and  $(\eta/s)/(\sigma_e/T)$ , respectively, is calculated from PLSM as a function of temperature. All these quantities are dimensionless. This should allow checking the possible scenarios when QGP approaches the phase transition and when the confinement dynamics becomes dominant. There is an independent behavior, when the quarks and gluons become deconfined and deform the new-state-of-matter, the QGP. Both quantities  $(\xi/s)/(\sigma_e/T)$  and  $(\eta/s)/(\sigma_e/T)$  are conjectured to give estimation for the deviation from the predicted values, which would be utilized as signatures of the unknown properties of QGP [28].

In [28], it is found that the temperature dependence of the ratio  $(\eta/s)/(\sigma_e/T)$  is independent of the strong running coupling,  $\alpha_s$  [28]. As the gluons are not electrically charged, the ratio could be regulated by relative strength and chemical composition of QGP [28] at very high temperature ( $5-10$ )  $T_c$  [28]. To the authors' best knowledge, not like  $(\eta/s)/(\sigma_e/T)$  [81], the  $(\xi/s)/(\sigma_e/T)$  is not yet calculated in lattice QCD.

#### IV. CONCLUSIONS AND OUTLOOK

The studying of transport properties is an effective aspect of characterizing the strongly interacting matter. When the system is perturbed from its equilibrium, the transport properties, such as bulk viscosity  $\xi$ , shear viscosity  $\eta$ , electric conductivity  $\sigma_e$  and thermal conductivity  $\kappa$ , play an essential role in defining the system of interest. For completeness, we mention that another transport coefficient

which plays an important role in the hydrodynamical evolution of the strongly interacting QCD matter especially around phase transition, is the ratio of bulk viscosity to the thermal entropy,  $\eta/s$ .

We have employed PLSM in order to study the transport coefficients in hadronic and partonic systems. In doing this, we have introduced various thermodynamical quantities such as trace anomaly, speed of sound and specific heat. Also, the first two higher-order moments, the particle number multiplicity and the particle number susceptibility contribute to the estimation of the transport coefficients. The quark decay widths and their relaxation time are estimated from DQPM. All these quantities are needed in describing the fundamental transport coefficients.

We find that the PLSM fits well with the results of lattice QCD calculations, especially from Hot-QCD collaboration. The subtracted chiral condensates and the deconfinement order parameters are in good agreement with each other. For instance, they confirm the steeper drop around the phase transition. Pure gluonic potential and the absence of gluon interaction are two characteristics of LSM. With introducing Polyakov-loop corrections to the LSM approach, we are able to compare the results with the same lattice data for trace anomaly at different quark flavor blind Yukawa coupling  $g = 6.5$  and  $10.5$ .

Also, the temperature dependence of the speed of sound and the specific heat downward the Stefan–Boltzmann limit are compared with the lattice results. The peaks in both curves refer to a fast change in the thermal rate in the energy density. The particle number multiplicity and particle number susceptibility at fixed different baryon chemical potential are compared with the corresponding Stefan–Boltzmann limits. We conclude that an increase in the baryon chemical potential seems to reduce the idealization of the system as the one with massless gluonic or fermions. We also find that the PLSM is not able to reproduce the lattice QCD equations of state. This is because of the degrees of freedom, which should not be sufficient near  $T_c$ . Furthermore, there is no explicit control on the color degrees of freedom and on their contributions to the thermodynamical potential. The fit parameters likely change according to the degrees of freedom. Here, we focus the discussion to the estimation of the transport coefficients, only. In a future work, we plan to update the model’s parameters according to the most recent lattice QCD simulations.

We have estimated the electric conductivity for a system, in which quarks and gluons are conjectured to scatter elastically and inelastically. This allows estimating their relaxation time and decay width. We find a good agreement with a relativistic version of the Drude formula for the electric conductivity. We have deduced the dimensionless electric conductivity and confronted it with the recent lattice QCD and found a good agreement. An irradiation occurring in the system has been considered. In calculating the heat conductivity, an irradiation is conjectured to take place in the system. This has been taken into consideration. The results are comparable with the QCD-like models. The gap

difference between the ratio of electric and thermal conductivities increases with increasing temperature, especially at  $T > T_c$ . There are no lattice QCD results to compare with.

The bulk viscosity which is related to various thermodynamical quantities, is calculated from the Kubo's formula. This quantity is strongly related to the phase transition and response to the instability in the hydrodynamic flow of the system. The shear viscosity has been estimated from the speed of sound and the bulk viscosity. The ratio of shear viscosity to the electric conductivity was compared with the available results of lattice QCD calculations. The agreement is very convincing. We conclude that PLSM is able to reproduce the lattice QCD calculations.

We have argued that the ratio of bulk and shear viscosities (normalized to the thermal entropy) and the electric conductivity,  $(\xi/s)/(\sigma_e/T)$  and  $(\eta/s)/(\sigma_e/T)$ , would favor or disfavor the possible phenomenological scenarios from PLSM (present work) or PNJL or DQPM, especially QGP cools down to  $T_c$ . There are different independent behaviors referring to essential properties of QGP. These are regulated by relative strength and chemical composition of the QGP. The transport coefficients for different QCD-like models show a clear dependence on temperature and baryon chemical potential. The results of the transport properties are basic ingredients on studying hot and dense matter.

**Acknowledgements.** The work was partly supported by ARE-JINR joint cooperation agreement and partly by the World Laboratory for Cosmology and Particle Physics (WLCAPP), <http://wlcapp.net/>. A.T. is very grateful to Elena Bratkovskaya and Rudy Marty for the NJL and DQPM calculations and would like to thank Ernst-Michael Ilgenfritz and David Blaschke for the extraordinary help in getting this script published in JINR-preprint.

## REFERENCES

1. *Gross D.J., Wilczek F.* "Ultraviolet behavior of non-Abelian gauge theories". Phys. Rev. Lett. 1973. V. 30. P. 1343.
2. *Politzer H.D.* "Reliable perturbative results for strong interactions?" Phys. Rev. Lett. 1973. V. 30. P. 1346.
3. *Gyulassy M., McLerran L.* "New forms of QCD matter discovered at RHIC". Nucl. Phys. A. 2005. V. 750. P. 30.
4. *Fukushima K.* "Chiral effective model with the Polyakov loop". Phys. Lett. B. 2004. V. 591. P. 277.
5. *Fukushima K.* "Phase diagrams in the three-flavor Nambu–Jona-Lasinio model with the Polyakov Loop". Phys. Rev. D. 2008. V. 77. P. 114028.
6. *Ratti C., Thaler M., Weise W.* "Phases of QCD: Lattice thermodynamics and a field theoretical model". Phys. Rev. D. 2005. V. 73. P. 014019.
7. *Schaefer B.-J., Wambach J.* "Susceptibilities near the QCD (tri)critical point". Phys. Rev. D. 2007. V. 75. P. 085015.

8. *Schaefer B.-J., Pawłowski J.M., Wambach J.* "The phase structure of the Polyakov–quark-meson model". *Phys. Rev. D.* 2007. V. 76. P. 074023.
9. *Schaefer B.-J., Wagner M.* "On the QCD phase structure from effective models". *Nucl. Phys.* 2009. V. 62. P. 381.
10. *Schaefer B.-J., Wagner M., Wambach J.* "QCD thermodynamics with effective models". *PoS CPOD.* 2009. V. 017.
11. *Thaler M.A., Schneider R.A., Weise W.* "Quasiparticle description of hot QCD at finite quark chemical potential". *Phys. Rev. C.* 2004. V. 69. P. 035210.
12. *Letessier J., Rafelski J.* "QCD equations of state and the QGP liquid model". *Phys. Rev. C.* 2003. V. 67. P. 031902.
13. *Bluhm M., Kampfer B., Soff G.* "The QCD equation of state near  $T(c)$  within a quasiparticle model". *Phys. Lett. B.* 2005. V. 620. P. 131.
14. *Mao H., Jin J., Huang M.* "Phase diagram and thermodynamics of the Polyakov linear-sigma model with three quark flavors". *J. Phys. G.* 2010. V. 37. P. 035001.
15. *Tawfik A., Magdy N., Diab A.* "Polyakov linear SU(3) sigma model: Features of higher order moments in dense and thermal hadronic medium". *Phys. Rev. C.* 2014. V. 89. P. 055210.
16. *Schaefer B.J., Wagner M.* "The three-flavor chiral phase structure in hot and dense QCD matter". *Phys. Rev. D.* 2009. V. 79. P. 014018.
17. *Gupta U., Tiwari V.* "Meson masses and mixing angles in 2+1 flavor Polyakov quark meson sigma model and symmetry restoration effects". *Phys. Rev. D.* 2010. V. 81. P. 054019;  
*Tiwari V.* "Comparing symmetry restoration trends for meson masses and mixing angles in the QCD-like three quark flavor models". *Phys. Rev. D.* 2013. V. 88. P. 074017.
18. *Tawfik A., Diab A.* "Polyakov SU(3) extended linear  $\sigma$ -model: Sixteen mesonic states in chiral phase-structure". *Phys. Rev. C.* 2015. V. 91. P. 015204.
19. *Tawfik A., Magdy N.* "SU(3) Polyakov linear sigma-Model in an external magnetic field". *Phys. Rev. C.* 2014. V. 90. P. 015204.
20. *Tawfik A., Magdy N.* "Thermodynamics and higher order moments in SU(3) linear  $\sigma$ -model with gluonic quasiparticles". *J. Phys. G.* 2015. V. 42. P. 015004.
21. *Denicol G.S. et al.* "Derivation of transient relativistic fluid dynamics from the Boltzmann equation". *Phys. Rev. D.* 2012. V. 85. P. 114047.
22. *Denicol G.S. et al.* "Derivation of fluid dynamics from kinetic theory with the 14-moment approximation". *Eur. Phys. J. A.* 2012. V. 48. P. 170.
23. *Denicol G.S., Koide T., Rischke D.H.* "Dissipative relativistic fluid dynamics: A new way to derive the equations of motion from kinetic theory". *Phys. Rev. Lett.* 2010. V. 105. P. 16250.
24. *Marty R. et al.* "Transport coefficients from the Nambu–Jona-Lasinio model for  $SU(3)_f$ ". *Phys. Rev. C.* 2013. V. 88. P. 045204.
25. *Berrehrah H. et al.* "Transport coefficients of heavy quarks around  $T_c$  at finite quark chemical potential". *Phys. Rev. C.* 2014. V. 90. P. 051901.
26. *Li Bao-Chun, Huang Mei.* "Thermodynamic properties and bulk viscosity near phase transition in the  $Z(2)$  and  $O(4)$  models". *Phys. Rev. D.* 2009. V. 80. P. 034023.

27. *Ozvenchuk V. et al.* "Shear and bulk viscosities of strongly interacting infinite parton-hadron matter within the parton-hadron-string dynamics transport approach". *Phys. Rev. C.* 2013. V. 87. P. 064903.
28. *Puglisi A., Plumari S., Greco V.* "Shear viscosity  $\eta$  to electric conductivity  $\sigma_{el}$  ratio for the Quark-Gluon Plasma". arXiv:1407.2559 [hep-ph].
29. *Lenaghan J.T., Rischke D.H., Schaffner-Bielich J.* "Chiral symmetry restoration at nonzero temperature in the  $SU(3)(r) \times SU(3)(l)$  linear sigma model". *Phys. Rev. D.* 2000. V. 62. P. 085008.
30. *Scavenius O. et al.* "Chiral phase transition within effective models with constituent quarks". *Phys. Rev. C.* 2001. V. 64. P. 045202.
31. *Polyakov A.M.* "Thermal properties of gauge fields and quark liberation". *Phys. Lett. B.* 1978. V. 72. P. 477.
32. *Susskind L.* "Lattice models of quark confinement at high temperature". *Phys. Rev. D.* 1979. V. 20. P. 2610.
33. *Gell-Mann M., Levy M.* "The axial vector current in beta decay". *Nuovo Cimento.* 1960. V. 16. P. 53.
34. *Gasiorowicz S., Geffen D.A.* "Effective Lagrangians and field algebras with chiral symmetry". *Rev. Mod. Phys.* 1969. V. 41. P. 531.
35. *Kovacs P., Szep Z.* "The critical surface of the  $SU(3)_L \times SU(3)_R$  chiral quark model at nonzero baryon density". *Phys. Rev. D.* 2007. V. 75. P. 025015.
36. *Rossner S., Ratti C., Weise W.* "Polyakov loop, diquarks and the two-flavour phase diagram". *Phys. Rev. D.* 2007. V. 75. P. 034007.
37. *Kapusta J.I., Gale C.* "Finite-temperature field theory: Principles and applications". Cambridge University Press, UK, 2006.
38. *Cheng M. et al.* "The QCD equation of state with almost physical quark masses". *Phys. Rev. D.* 2008. V. 77. P. 014511.
39. *Cheng S. et al.* "Equation of state for physical quark masses". *Phys. Rev. D.* 2010. V. 81. P. 054504.
40. *Haas L.M. et al.* "Improved Polyakov-loop potential for effective models from functional calculations". *Phys. Rev. D.* 2013. V. 87. P. 076004.
41. *Bazavov A. (HotQCD Collaboration.)* "Chiral transition temperature and aspects of deconfinement in 2+1 flavor QCD with the HISQ/tree action". *PoS LATTICE2011,* 2011. V. 182.
42. *Bazavova A. et al.* "Equation of state and QCD transition at finite temperature". *Phys. Rev. D.* 2009. V. 80. P. 014504.
43. *Orginos K., Toussaint D.* "Testing improved actions for dynamical Kogut-Susskind quarks". *Phys. Rev. D.* 1999. V. 59. P. 014501;  
*Lepage G.P.* "Flavor symmetry restoration and Symanzik improvement for staggered quarks". *Phys. Rev. D.* 1999. V. 59. P. 074502;  
*Orginos K., Toussaint D., Sugar R.L. (MILC Collaboration.)* "Variants of fattening and flavor symmetry restoration". *Phys. Rev. D.* 1999. V. 60. P. 054503.
44. *Heller U.M., Karsch F., Sturm B.* "Improved staggered fermion actions for QCD thermodynamics". *Phys. Rev. D.* 1999. V. 60. P. 114502.

45. Peikert A. *et al.* "Staggered fermion actions with improved rotational invariance". Nucl. Phys. Proc. Suppl. 1998. V.63. P.895.
46. Levai P., Heinz U. "Massive gluons and quarks and the equation of state obtained from SU(3) lattice QCD". Phys. Rev. C. 1997. V.57. P.1879.
47. Romatschke P. "Quasiparticle description of the hot and dense quark gluon plasma". hep-ph/0312152.
48. Peshier A. "Hard gluon damping in hot QCD". Phys. Rev. D. 2004. V.70. P.034016; Peshier A., Kampfer B., Soff G. "From QCD lattice calculations to the equation of state of quark matter". Phys. Rev. D. 2002. V.66. P.094003; Peshier A., Cassing W. "The hot non-perturbative gluon plasma is an almost ideal colored liquid". Phys. Rev. Lett. 2005. V.94. P.172301.
49. Aoki Y. *et al.* "The QCD transition temperature: Results with physical masses in the continuum limit". Phys. Lett. B. 2006. V.643. P.46; Borsanyi S. *et al.* "Is there still any  $T_c$  mystery in lattice QCD? Results with physical masses in the continuum limit III". JHEP. 2010. V.1009. P.073.
50. Tawfik A. "Constant trace anomaly as a universal condition for the chemical freeze-out". Phys. Rev. C. 2013. V.88. P.035203.
51. Bazavov A. *et al.* "Equation of state in (2 + 1)-flavor QCD". Phys. Rev. D. 2014. V.90. P.094503.
52. Borsanyi Szabolcs *et al.* " $N_f = 2 + 1$  flavor equation of state". JHEP. 2010. V.1011. P.077.
53. Reif F. "Fundamentals of statistical and thermal physics". McGraw-Hill, New York, 1965.
54. Cassing W. "Electrical conductivity of hot QCD matter". Phys. Rev. Lett. 2013. V.110. P.182301.
55. Israel W., Stewart J.M. "Transient relativistic thermodynamics and kinetic theory". Ann. Phys. (N. Y.) 1979. V.118. P.341.
56. de Groot S., van Leeuwen W., van Weert C. "Relativistic kinetic theory: Principles and applications". North-Holland, Amsterdam, 1980.
57. Greif M. "Derivation of transient relativistic fluid dynamics from the Boltzmann equation". Phys. Rev. D. 2012. V.85. P.114047.
58. Greif M. "Heat conductivity in relativistic systems investigated using a partonic cascade". Phys. Rev. E. 2013. V.87. P.033019.
59. Donnelly S.E., Birtcher R.C. "Radiation damage from single heavy ion impacts on metal surface". Proc. SPIE 3413, Materials Modification by Ion Irradiation, 174, September 17, 1998.
60. Heiselberg H., Pethick C.J. "Transport and relaxation in degenerate quark plasmas". Phys. Rev. D. 1993. V.48. P.2916.
61. Sasaki C., Redlich K. "Transport coefficients near chiral phase transition". Nucl. Phys. A. 2010. V.832. P.62.
62. Gupta S. "The electrical conductivity and soft photon emissivity of the QCD plasma". Phys. Lett. B. 2004. V.597. P.57.

63. *Amato A. et al.* "Electrical conductivity of the quark–gluon plasma across the deconfinement transition". *Phys. Rev. Lett.* 2013. V. 111. P. 172001.
64. *Ding H.-T.* "Thermal dilepton rate and electrical conductivity: An analysis of vector current correlation functions in quenched lattice QCD". *Phys. Rev. D.* 2011. V. 83. P. 034504.
65. *Brandt B. B. et al.* "Thermal correlators in the  $\rho$  channel of two-flavor QCD". *J. High Energy Phys.* 2013. V. 1303. P. 100.
66. *Stephanov M. A.* "QCD phase diagram: An overview". *PoS LAT2006.* 2006. V. 024.
67. *Stephanov S. et al.* "The chiral and deconfinement crossover transitions: PNJL model beyond mean field". *Nucl. Phys. A.* 2008. V. 814. P. 118.
68. *Karsch F., Kharzeev D., Tuchin K.* "Universal properties of bulk viscosity near the QCD phase transition". *Phys. Lett. B.* 2008. V. 663. P. 217.
69. *Meyer H. B.* "A calculation of the shear viscosity in SU(3) gluodynamics". *Phys. Rev. D.* 2007. V. 76. P. 101701;  
*Meyer H. B.* "A calculation of the bulk viscosity in SU(3) gluodynamics". *Phys. Rev. Lett.* 2008. V. 100. P. 162001.
70. *Sakai S., Nakamura A.* "Lattice calculation of the QGP viscosities: Present results and next project". *PoS LAT2007.* 2007. V. 221.
71. *Nakamura A., Sakai S.* "Transport coefficients of gluon plasma". *Phys. Rev. Lett.* 2005. V. 94. P. 072305.
72. *Benincasa P.* "Sound waves in strongly coupled non-conformal gauge theory plasma". *Int. J. Mod. Phys. A.* 2005. V. 20. P. 6298.
73. *Hosoya A., Sagakami M. A., Takao M.* "Nonequilibrium thermodynamics in field theory: Transport coefficients". *Annals Phys.* 1984. V. 154. P. 299.
74. *Horsley R., Schoenmaker W.* "Quantum field theories out of thermal equilibrium. 1. General considerations". *Nucl. Phys. B.* 1987. V. 280. P. 716.
75. *Paech K., Pratt S.* "Origins of bulk viscosity in relativistic heavy ion collisions". *Phys. Rev. C.* 2006. V. 74. P. 014901.
76. *Torrieri G., Mishustin I.* "Instability of Boost-invariant hydrodynamics with a QCD inspired bulk viscosity". *Phys. Rev. C.* 2008. V. 78. P. 021901;  
*Torrieri G., Tomasik B., Mishustin I.* "Bulk viscosity driven clusterization of quark–gluon plasma and early freeze-out in relativistic heavy-ion collisions". *Phys. Rev. C.* 2008. V. 77. P. 034903.
77. *Khvorostukhin A. S., Toneev V. D., Voskresensky D. N.* "Viscosity coefficients for hadron and quark–gluon phases". *Nucl. Phys. A.* 2010. V. 845. P. 106;  
*Khvorostukhin A. S., Toneev V. D., Voskresensky D. N.* "Relaxation time ansatz and shear and bulk viscosities of gluon matter". *Phys. Rev. C.* 2011. V. 84. P. 035202.
78. *Cassing W., Bratkovskaya E. L.* "Parton transport and hadronization from the dynamical quasiparticle point of view". *Phys. Rev. C.* 2008. V. 78. P. 034919.
79. *Konchakovski V. P. et al.* "Azimuthal anisotropies for Au+Au collisions in the parton-hadron transient energy range". *Phys. Rev. C.* 2012. V. 85. P. 044922;  
*Konchakovski V. P. et al.* "Collective properties of nucleus–nucleus collisions from AGS to LHC energies". *J. Phys. Conf. Ser.* 2012. V. 389. P. 012015.

80. *Kovtun P. K., Son D. T., Starinets A. O.* "Viscosity in strongly interacting quantum field theories from black hole physics". *Phys. Rev. Lett.* 2005. V. 94. P. 111601.
81. *Kaczmarek O. et al.* "Thermal dilepton rates from quenched lattice QCD". *PoS ConfinementX*, 2012. V. 185;  
*Brandt B. B. et al.* "Two-flavour lattice QCD correlation functions in the deconfinement transition region". *PoS ConfinementX*, 2012. V. 186;  
*Aarts G. et al.* "Spectral functions at small energies and the electrical conductivity in hot, quenched lattice QCD". *Phys. Rev. Lett.* 2007. V. 99. P. 022002;  
*Aarts G.* "Transport and spectral functions in high-temperature QCD". *PoS LAT2007*. 2007. V. 001.

Received on February 2, 2015.

Редактор *Э. В. Ивашкевич*

Подписано в печать 13.03.2015.

Формат 60 × 90/16. Бумага офсетная. Печать офсетная.

Усл. печ. л. 1,81. Уч.-изд. л. 2,64. Тираж 325 экз. Заказ № 58494.

Издательский отдел Объединенного института ядерных исследований  
141980, г. Дубна, Московская обл., ул. Жолио-Кюри, 6.

E-mail: [publish@jinr.ru](mailto:publish@jinr.ru)

[www.jinr.ru/publish/](http://www.jinr.ru/publish/)